Inorganic Chemistry

Article

pubs.acs.org/IC

Synthesis, Characterization, X-ray Crystal Structure, DFT Calculations, and Catalytic Properties of a Dioxidovanadium(V) Complex Derived from Oxamohydrazide and Pyridoxal: A Model Complex of Vanadate-Dependent Bromoperoxidase

Chandrima Das,[†] Piyali Adak,[†] Satyajit Mondal,[†] Ryo Sekiya,[‡] Reiko Kuroda,[‡] Serge I. Gorelsky,*[,⊥] and Shyamal Kumar Chattopadhyay*[,†]

[†]Department of Chemistry, Indian Institute of Engineering Science and Technology, Shibpur, Howrah 711 103, India

[‡]Department of Life Sciences, Graduate School of Arts and Sciences, The University of Tokyo, Komaba, Meguro-ku, Tokyo 153-8902 Japan

[⊥]Centre for Catalysis Research and Innovation, University of Ottawa, Ottawa, Ontario, Canada K1N 6N5,

Supporting Information

ABSTRACT: A vanadium(V) complex with the formula $[Et_3NH][V^VO_2(sox\text{-}pydx)]$ with a new tridentate ligand 2-[2-[[3-hydroxy-5-(hydroxymethyl)-2-methylpyridin-4-yl]methylene]-hydrazinyl]-2-oxoacetamide (soxH-pydxH), obtained by condensation of oxamohydrazide and pyridoxal (one of the forms of vitamin B_6), has been synthesized. The compound was characterized by various analytical and spectroscopic methods, and its structure was determined by single-crystal X-ray diffraction technique. Density functional theory (DFT) and time-dependent DFT calculations were used to understand the electronic structure of the complex and nature of the electronic transitions observed in UV−vis spectra. In the complex, vanadium(V) is found to be pentacoordinated with two oxido ligands and a bianionic tridentate ONO-donor ligand. The vanadium center has square-pyramidal geometry with an axial oxido ligand, and the equatorial positions are occupied by another oxido ligand and a phenolato oxygen, an imine nitrogen, and a deprotonated amide oxygen of the hydrazone ligand. A DFT-optimized structure of the complex shows very similar metrical parameters as determined by X-ray crystallography. The O_4N coordination environment of vanadium and the hydrogen-bonding abilities of the pendant amide moiety have a strong resemblance with the vanadium center in bromoperoxidase enzyme. Bromination experiments using H_2O_2 as the oxidizing agent, with model substrate phenol red, and the vanadium complex as a catalyst show a remarkably high value of k_{cat} equal to 26340 h^{-1}. The vanadium compound also efficiently catalyzes bromination of phenol and salicylaldehyde as well as oxidation of benzene to phenol by H_2O_2.

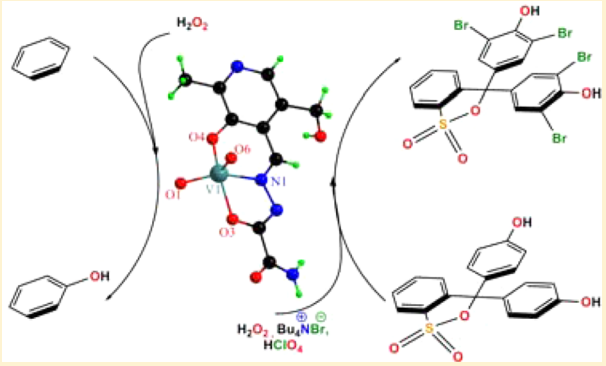

INTRODUCTION

The discovery of vanadium-dependent bromoperoxidase in marine algae,[1−3] some lichens,[4,5] and fungi,[6−12] which is used for the catalytic synthesis of organobromo compounds, has evoked interest in model studies of this enzyme.[13−23] It is believed that the organobromo natural products are used by the marine organisms for self-defense against predators.[3] Besides, the organobromo compounds are also known to possess antimicrobial and anticancer properties, which make them potential candidates for medicinal applications.[3,24,25] It is now established that in the resting state the bromoperoxidase enzyme contains vanadium(V) in a trigonal-bipyramidal coordination geometry with three nonprotein oxido groups in the trigonal plane and axial coordination by N^{ε} of a histidine imidazole and an OH group.[6,7,24,26] In the active state, which requires the presence of H_2O_2, a square-pyramidal monoperoxovanadium(V) complex is formed, where η^2-peroxide, N^{ε} (histidine), and oxido/hydroxo groups occupy the square plane and an oxido ligand occupies the axial site (Chart 1).[24,27−29] There is extensive hydrogen bonding between the coordinated oxido/hydroxo and peroxo ligands and amino acid residues from protein side chains.[23,24,30] A change of the oxidation state of the vanadium center has not been observed during the catalytic turnover.[31−33] The vanadium(V) center acts as a strong Lewis acid to activate the peroxo group, which then undergoes nucleophilic attack by bromide to form the reactive "Br^+" intermediate (most likely a $HOBr/Br_2/Br_3^-$ species).[31,34] The reactive "Br^+" intermediate, in turn, electrophilically attacks suitable organic substrates to

Received: May 24, 2014
Published: October 16, 2014

   dx.doi.org/10.1021/ic501216d | Inorg. Chem. 2014, 53, 11426−11437

Chart 1. Vanadium Chloroperoxidase Enzyme in Its Native Form and in a Peroxo-Bound Form[8,27,36]

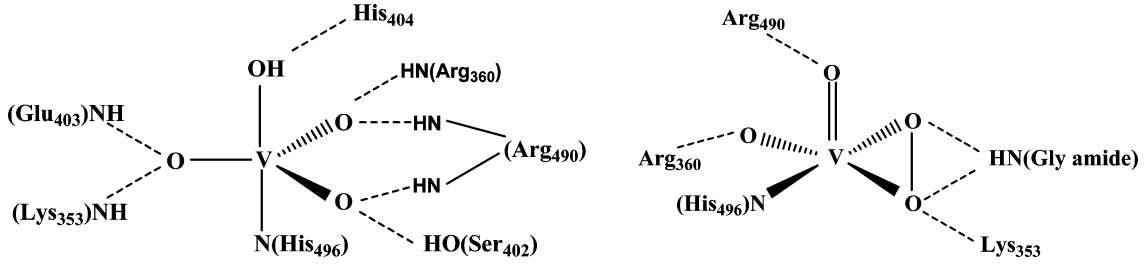

form brominated organic compounds. The peroxovanadium(V) form of the related chloroperoxidase enzyme has been structurally characterized for the fungi *Curvularia inaequalis*.[8,35−37] Single-crystal X-ray structures of quite a few model peroxovanadium(V) complexes capable of oxidative halogenation in the presence of H_2O_2 are also known.[30−32,34,38] The peroxo form of the enzyme is also capable of enantioselective oxidation of organic sulfides to sulfoxides.[39−43]

Vanadium complexes are also capable of oxidizing a variety of other organic substrates, e.g., epoxidation of alkenes and allyl alcohols, hydroxylation of alkenes and arenes, oxidation of primary and secondary alcohols to corresponding aldehydes and ketones, etc.[44,45] Although quite a few structural and/or functional model complexes of the bromoperoxidase enzyme are known in the literature,[27,30−32,34,44−50] it still appears that an understanding of the structural and electronic factors needed for predicting the stability and activity of model vanadium complexes during the catalytic cycle is lacking. Hence, a search for new vanadium complexes that mimic the enzyme activity and an understanding of their key structural and electronic features are very much desired. In this paper, we report a new vanadium(V) complex that exhibits bromoperoxidase activity with phenol, phenol red, and salicylaldehyde as substrates. The catalytic activity of the complex for oxidation of benzene to phenol by H_2O_2 is also reported.

EXPERIMENTAL SECTION

Physical Methods and Materials. Pyridoxal hydrochloride, oxamohydrazide (semioxamazide), and $VOSO_4{\cdot}H_2O$ were obtained from Aldrich, and triethylamine was purchased from E. Merck. All other chemicals and solvents were of reagent grade and were used as such, while solvents for spectroscopic and cyclic voltammetry (CV) studies were of high-performance liquid chromatographic grade obtained from Merck or Aldrich. Elemental analyses were performed on a PerkinElmer 2400 carbon, hydrogen, and nitrogen analyzer. IR spectra were recorded as KBr pellets on a Jasco FT-IR-460 spectrophotometer. UV−vis spectra were recorded using a Jasco V-530 spectrophotometer. CV and differential pulse voltammetry (DPV) experiments were carried out using a CH1106A potentiostat. A three-electrode configuration, with a glassy carbon working electrode, a platinum auxiliary electrode, a Ag/AgCl-saturated KCl reference electrode, and TEAP as the supporting electrolyte, was used. Under our experimental conditions, a ferrocene/ferrocenium couple was observed at E_0 (ΔE_p) = 0.48 V (100 mV). ^{1}H NMR spectra were recorded on a Bruker AVANCE DPX 300 MHz spectrometer using $Si(CH_3)_4$ as the internal standard. Electrospray ionization mass spectrometry (ESI-MS) spectra of the samples were recorded on a JEOL JMS 600 instrument. The products of the catalytic reactions were identified and quantified by using a Varian CP-3800 gas chromatograph equipped with a flame ionization detector.

Synthesis of the Ligand 2-[2-[[3-Hydroxy-5-(hydroxymethyl)-2-methylpyridin-4-yl]methylene]hydrazinyl]-2-oxoacetamide (soxH-pydxH). To prepare the tridentate ligand, pyridoxal hydrochloride (0.406 g, 2 mmol) was dissolved in 40 mL of methanol and the pH was set to 6.5−7.0 by the addition of concentrated KOH. Oxamohydrazide (semioxamazide; 0.206 g, 2 mmol) dissolved in water (5 mL) was added drop by drop to the pyridoxal suspension. The solution was stirred for 3 h, and a yellow precipitate was obtained. The residue was filtered and washed with ice-cold methanol and diethyl ether. Yield: 472 mg (94%). Anal. Calcd for $C_{10}H_{12}N_4O_4$ (MW 252.23): C, 47.60; H, 4.76; N, 22.21. Found: C, 47.35; H, 4.83; N, 22.40. ^{1}H NMR (DMSO-d_6): δ 12.85 (1H, s), 12.04 (1H, s), 9.09 (1H, s), 8.39 (1H, s), 8.02 (2H, d), 5.37 (1H, s), 4.59 (2H, s), 2.42 (3H, s) (Figure S1 in the Supporting Information, SI). ^{13}C NMR (DMSO-d_6): δ 161.45, 157.34, 151.33, 149.45, 147.43, 137.89, 133.59, 120.87, 58.90, 18.71 (Figure S2 in the SI). Electronic spectrum in a *N*,*N*-dimethylformamide (DMF) solution with λ_{max}/nm (ε_{max}/M^{-1} cm^{-1}): 340 (5110), 296 (10340). Selected IR bands (cm^{-1}): 3412 ($\nu^{asym}{}_{NH_2}$), 3258 ($\nu^{sym}{}_{NH_2}$), 3165 (ν_{O-H}), 3041 (ν_{N-H}), 1681 ($\nu_{C=O}$), 1595 sh ($\nu_{C=N}$).

Synthesis of Complex [Et$_3$NH][V^{V}O$_2$(sox-pydx)] (1). To a vigorously stirred methanolic solution (15 mL) of the ligand soxH-pydxH (251 mg, 1 mmol) was added Et_3N (202 mg, 2 mmol). A solution of $VOSO_4{\cdot}H_2O$ (180 mg, 1 mmol) in methanol (10 mL) was added dropwise to the above solution. The solution turned chocolate brown. The mixture was stirred at room temperature for 3 h and then filtered. The yellowish-brown residue, containing the crude complex, was washed with cold methanol and then dried over fused calcium chloride. The complex was recrystallized from methanol. The filtrate was allowed to evaporate slowly at room temperature. After 2 days, yellow, square-shaped, shiny crystals of complex **1** suitable for X-ray diffraction studies were obtained. Yield: 356 mg (82%). Anal. Calcd for $C_{16}H_{26}N_5O_6V$ (MW 435.36): C, 44.10; H, 5.97; N, 16.08. Found: C, 44.07; H, 5.95; N, 15.98. ESI-MS (positive-ion mode): *m*/*z* 378.78 [({VO_2(sox-pydx)} + 2Na)$^+$ (100%)] (Figure S3 in the SI). ESI-MS (negative-ion mode): *m*/*z* 333.14 [{VO_2(sox-pydx)}$^-$ (100%)] (Figure S4 in the SI). ^{1}H NMR (DMSO-d_6): δ 9.28 (1H, s), 7.75 (2H, s), 7.55 (1H, s), 5.40 (1H, s), 4.66 (2H, s), 3.09 (7H, s), 2.34 (3H, s), 1.16 (9H, s) (Figure S4 in the SI). Electronic spectrum in a DMF solution with λ_{max}/nm (ε_{max}/M^{-1} cm^{-1}): 325 (9770), 411 (5800). Selected IR bands (cm^{-1}): 3468 ($\nu^{asym}{}_{NH_2}$), 3272 (br, $\nu^{sym}{}_{NH_2}$ + ν_{O-H}), 3022 (ν_{N-H}),1690 ($\nu_{C=O}$), 1612 ($\nu_{C=N}$), 1446 (ν_{C-O}), 899 and 953 ($\nu_{O=V=O}$) (Figure S6 in the SI).

X-ray Crystallography. Single-crystal X-ray data were collected for **1** on a Bruker SMART APEXCCD diffractometer at 103(2) K, using Mo Kα radiation (0.71073 Å). Data were corrected for absorption effects using the numerical method *SADABS*,[51] solved by direct methods, and refined by full-matrix least squares on F^2 using *SHELX-97*.[52] The non-hydrogen atoms were refined with anisotropic displacement parameters. All hydrogen atoms were placed at calculated positions and refined as riding atoms using isotropic displacement parameters. A summary of the crystallographic data is presented in Table 1. Important bond distances and bond angles are collected in Table 2. Crystallographic data have been deposited at the Cambridge Crystallographic Data Centre as deposition number 1004534.

Density Functional Theory (DFT) Calculations. All DFT calculations were performed using the *Gaussian 09* package[53] using the B3LYP hybrid functional[54] and the TZVP basis set[55] for all atoms. The structures of all species were optimized without any constraints in

dx.doi.org/10.1021/ic501216d | *Inorg. Chem.* 2014, 53, 11426−11437

Table 1. Crystal Data and Refinement Details of 1

formula	$C_{16}\ H_{26}\ N_5\ O_6V$
fw	435.36
cryst size (mm^3)	0.37 × 0.24 × 0.07
temperature (K)	103(2)
cryst syst	triclinic
space group	$P\bar{1}$
a (Å)	8.2552(7)
b (Å)	10.1594(9)
c (Å)	12.645(1)
α (deg)	68.371(2)
β (deg)	83.963(2)
γ (deg)	81.757(2)
d_{cal}	1.484
Z	2
μ (mm^{-1})	0.553
F(000)	456.0
total reflns	6018
unique reflns	4238
obsd data [$I > 2\sigma(I)$]	3719
R(int)	0.0286
R1, wR2 [$I > 2\sigma(I)$]	0.0509, 0.1295
R1, wR2 (all data)	0.0579, 0.1351

Table 2. Bond Distances (Å) and Angles (deg) for 1

bond lengths (Å)			
V1−O1	1.653(2)	V1−O6	1.617(2)
V1−O3	1.900(2)	V1−N1	2.156(2)
V1−O4	1.989(2)		
bond angles (deg)			
O1−V1−O3	96.13(8)	O6−V1−O4	101.57(8)
O1−V1−O4	91.31(8)	O1−V1−N1	143.57(8)
O3−V1−O4	146.48(8)	O3−V1−N1	81.31(7)
O6−V1−O1	108.72(9)	O4−V1−N1	73.59(7)
O6−V1−O3	106.77(9)	O6−V1−N1	106.75(8)

solution using water as a solvent and the SMD implicit solvation model.[56] The same level of theory with tight self-consistent-field convergence criteria was used for all other calculations. The converged wave functions were tested to confirm that they correspond to the ground-state potential energy surface (PES). Evaluation of the atomic charges and spin densities was performed using natural population analysis.[57] Analyses of the molecular orbitals in terms of fragment orbital contributions (based on the Mulliken population analysis, MPA)[58a] and Mayer[58b] and orbital occupancy perturbed bond order[58c] calculations were carried out using the *AOMix* program.[58d,e] Time-dependent DFT (TD-DFT) calculations were performed to calculate the absorption spectra. These spectra were simulated with the *SWizard* program,[59] revision 4.6, using pseudo-Voigt functions with a half-bandwidth, $\Delta_{1/2}$, of 3000 cm^{-1}.

Catalytic Study. The bromination of phenol red to bromophenol blue using complex **1** as a catalyst was studied by absorption spectroscopy. An aliquot of 30% H_2O_2 was added to a DMF solution of 0.1 mmol of catalyst, so that the final concentration of H_2O_2 in the reaction mixture was 1 mM. This was followed by the addition of $HClO_4$ (final concentration 2.0 mM) and 4.0 mmol of tetra-*N*-butylammonium bromide. Finally, 0.25 mmol of phenol red was added, and the solution was stirred at a constant temperature of 25 °C. Spectral measurements of aliquots withdrawn, and buffered at pH = 7.1 with an aqueous phosphate buffer, were taken at regular time intervals. The spectral data show the gradual disappearance of the 434 nm band and growth of the band of bromophenol blue at 590 nm, and the reaction was complete under the ambient conditions after ∼4 h.

Kinetic studies of the bromination of phenol red to bromophenol blue were carried out using complex **1** as a catalyst, by monitoring the increase in absorbance at 590 nm by the initial rate method. To a DMF solution of 0.01 mmol of catalyst were added under stirring 0.1 mM 30% H_2O_2, 0.2 mM $HClO_4$, and 0.4 mmol of tetra-*N*-butylammonium bromide, and the reaction mixture was thermostated at 25 °C. With an increase of the substrate (phenol red) concentration from 20 to 60 equiv with respect to the catalyst (0.01 mmol), the dependence of the rates on the substrate concentration was determined.

The dioxidovanadium complex **1** can also catalyze the oxidative bromination of salicylaldehyde as well as phenol using H_2O_2, KBr, and $HClO_4$ in an aqueous solution. To achieve an optimum reaction condition for the bromination reaction, the volumes of H_2O_2 and acid were varied. With salicylaldehyde as the substrate, for a fixed amount of substrate (5 mmol), 0.01 mmol of catalyst, 10 mmol of KBr, 30 mmol of H_2O_2, and 5 mmol of $HClO_4$ in an aqueous medium were found to be the optimum conditions, where the maximum amount of the substrate is converted to the desired product 5-bromosalicylaldehyde. To stop decomposition of the catalyst, 1 mmol portions of $HClO_4$ were added successively, during the course of the reaction every 1 h for 4 h.

For the catalytic study of oxidation of benzene by H_2O_2, aqueous H_2O_2 (25 mmol) and benzene (50 mmol) were taken in 5 mL of acetonitrile. Complex **1** (0.1 mmol) dissolved in a minimum volume of water was added to it. The reaction mixture was thermostated at 80 °C in an oil bath with stirring. After specific time intervals, small amounts of aliquots were withdrawn from the reaction mixture and analyzed by gas chromatography (GC).

Scheme 1. Synthesis of Complex 1

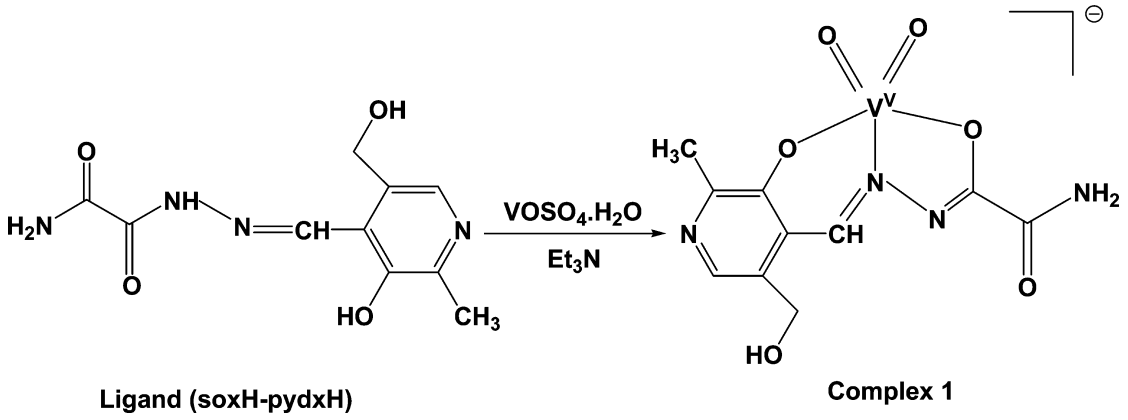

dx.doi.org/10.1021/ic501216d | *Inorg. Chem.* 2014, 53, 11426−11437

RESULTS AND DISCUSSION

Synthesis and Spectroscopic Characterization. It has been reported in the literature that the dioxidovanadium(V) complex of pyridoxal isonicotinoyl hydrazone shows bromoperoxidase mimicking activity.[46] Although no explanation was offered in the paper as to why the complex showed such activity, our own experience with pyridoxal Schiff base ligands[60] prompted us to believe that the hydrogen-bonding ability of the pyridoxal residue may play an important role in determining the bromoperoxidase mimicking ability, by stabilizing the catalyst−substrate complex. With this assumption, we thought that a vanadium(V) complex with a pyridoxal Schiff base of oxamohydrazide, with a pendant amide group, providing added hydrogen-bonding sites but less steric bulk compared to the pyridine ring of isonicotinoyl hydrazone, may be a better candidate for the exploration of model bromoperoxidase acitivity by complexation with VO_2^+. For this purpose, the ligand soxH-pydxH was synthesized by reacting methanolic solutions of neutral pyridoxal with oxamohydrazide at room temperature. Upon reaction of the ligand with vanadium sulfate in the presence of triethylamine in a methanol medium, the monoanionic vanadium(V) complex **1** was obtained with triethylammonium as the countercation (Scheme 1). In the free ligand, a sharp, relatively broad band at 1681 cm^{-1} is assigned to overlapping $\nu_{C=O}$ vibrations of the two carbonyl groups, whereas a shoulder at 1595 cm^{-1} is assigned to the $\nu_{C=N}$ vibration. The asymmetric stretching vibration ($\nu^{asym}_{NH_2}$) of the NH_2 moiety is located at 3412 cm^{-1}. Between 3260 and 3000 cm^{-1}, the free ligand shows a strong absorption envelope with broad peaks at 3258, 3165, and 3041 cm^{-1}, which are assigned to $\nu^{sym}_{NH_2}$, ν_{O-H}, and ν_{N-H}, respectively. The broad envelope indicates extensive hydrogen bonding involving multiple OH and NH functionalities. In the vanadium complex **1**, a $\nu^{asym}_{NH_2}$ vibration is observed at 3468 cm^{-1}, whereas the relatively broad peak at 3272 cm^{-1} is assigned to overlapping $\nu^{sym}_{NH_2}$ and ν_{O-H} (hydroxymethyl) vibrations. The bands at 3165 and 3041 cm^{-1} present in the free ligand are absent in the complex, whereas a new band observed at 3022 cm^{-1} is probably due to the ν_{N-H} vibration of the hydrogen-bonded triethylammonium group. The $\nu_{C=O}$ vibration of the pendant amide is observed in the complex at 1690 cm^{-1}, while the $\nu_{C=N}$ vibration is now located at 1612 cm^{-1}. A new band at 1446 cm^{-1} in the complex is assigned to the ν_{C-O} vibration,[31,32] while two strong vibrations at 899 and 953 cm^{-1} are assigned to the antisymmetric and symmetric stretching vibrations of the dioxovanadium(V) moiety (Figure S6 in the SI).

In the ^1H NMR spectra, the phenolic OH proton at 12.85 ppm, present in the ligand, is absent in the complex, whereas the aldimine proton undergoes a downfield shift from 9.09 ppm in the ligand to 9.29 ppm in the complex. The aromatic proton shifts upfield from 8.39 ppm in the ligand to 7.55 ppm in the complex. The methyl and methylene protons attached to the heterocyclic ring are observed at 2.42 and 4.59 ppm, respectively, in the ligand and at 2.34 and 4.66 ppm, respectively, in the complex.

The electronic spectrum of the ligand, recorded in a DMF solution, consists of an intense band at 340 nm, assigned to the $\pi \rightarrow \pi^*$ transition of the imine moiety, and another more intense transition at 296 nm, due to the $\pi \rightarrow \pi^*$ transition of the heterocyclic ring.[60] In the vanadium(V) complex, a strong band at 411 nm corresponds to the $\pi \rightarrow \pi^*$ transition of the ligand (see the TD-DFT section of the Results and Discussion section). The zinc(II) complex of the same ligand shows a band of comparable intensity at 427 nm (Figure S7 in the SI), supporting the above assignment of the band as a ligand-centered rather than a ligand-to-metal charge-transfer (LMCT) transition. Another strong band at 325 nm corresponds to a $\pi(L) \rightarrow d_\pi(V)$ LMCT transition (Figure 1).

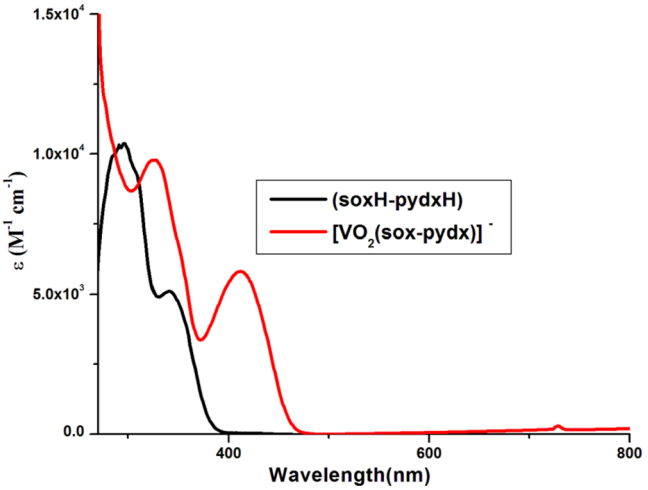

Figure 1. UV−vis spectra for the ligand soxH-pydxH and complex **1** in DMF at 298 K.

Description of the Structure. The molecular structure of the vanadium(V) complex is shown in Figure 2, and relevant

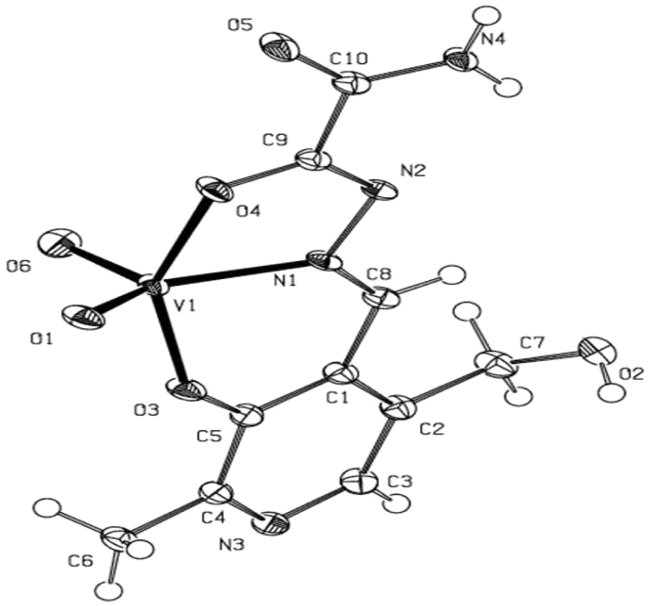

Figure 2. X-ray crystal structure of $[Et_3NH][VO_2(sox\text{-}pydx)]$. For clarity, only the anionic complex part is shown.

metal−ligand bond distances and angles are reported in Table 2. In the structure, the vanadium ion is in an O_4N-donor environment, arranged in a square-pyramidal geometry (Addison parameter[61] $\tau = 0.05$; $\tau = 0.00$ for a square pyramid and 1.00 for a trigonal bipyramid). The equatorial plane consists of O1, O3, O4, and N1 atoms, and the vanadium atom is displaced by 0.5212(4) Å from the plane toward the axial

dx.doi.org/10.1021/ic501216d | Inorg. Chem. 2014, 53, 11426−11437

oxygen O6. The metrical parameters are similar to those reported in the literature for monoanioinic vanadium(V) complexes in an O_4N-donor environment, which includes two oxido ligands.[46,62] The metal−ligand distances follow the order V═O (O1 and O6) < V−O$^-$ (O3 and O4) < V−N. The V═O and V−N distances in the present complex compare well with those of the choloroperoxidase enzyme from *C. inaequalis*, where the corresponding bond distances are 1.65 and 2.25 Å, respectively.[8] The pyridoxal ring nitrogen and the pendant hydroxymethyl group attached to it, as well as the uncoordinated amide moiety, participate in the formation of an extensive hydrogen-bonding network. The hydroxymethyl O2−H1 forms a complementary hydrogen bond with the oxido oxygen O1 of a neighboring unit (O2−H1···O1^{i}; symmetry code i = $-x$, $-y$, $1 - z$; Table S1 in the SI) to form a hydrogen-bonded dimer. Such dimers are then interconnected with each other by N4−H4···N3^{ii} (symmetry code ii = $-1 + x$, $1 + y$, z) by hydrogen bonds to form a one-dimensional chain along the [1, −1, 0] base vector. The triethylammonium cations in the crystal are hydrogen-bonded to the vanadium complex anions, where the coordinated amide oxygen O4 and the pendant amide oxygen O5 act as hydrogen-bond acceptors and the N5 of the triethylammonium ion acts as a hydrogen-bond donor (Figure S8 in the SI).

Electronic Structure. The DFT-optimized structure of the anionic $[V^VO_2(\text{sox-pydx})]^-$ complex reproduces the coordination environment of the central atom in the X-ray structure of the complex (Figure 2 and Table 2). The calculated V═O_{ax} and V═O_{eq} bond lengths are 1.631 and 1.639 Å, respectively, while the calculated V−O3, V−O4, and V−N1 bond lengths are 1.930, 2.015, and 2.209 Å, respectively. The O_{eq}−V−O_{ax} angle in the calculated structure (109.7°) also agrees well with the experimental value (108.7°). The lowest-energy structure from the DFT optimization contains the uncoordinated amide moiety (atoms C10, N4, and O5), which is rotated 180° around the C9−C10 bond relative to the X-ray structure. The energy minimum that contains the amide moiety with the same orientation as that in the X-ray structure has a slightly higher energy in solution (ΔE of 0.29 kcal mol^{-1} and $\Delta G_{298\ K}$ of 0.28 kcal mol^{-1}). However, this geometry can be stabilized by hydrogen bonding in the solid state, as observed in the X-ray structure. The rotation of the amide moiety around the C9−C10 bond has a low-energy barrier in solution ($\Delta E^{‡}$ of 3.4 kcal mol^{-1} and $\Delta G^{‡}_{298\ K}$ of 3.8 kcal mol^{-1}). Thus, the optimized structure in solution is consistent with the experimental X-ray structure of the complex in the solid state.

The frontier molecular orbitals (FMOs) of complex **1** are shown in Table 3 and Figure S9 in the SI. The three highest occupied molecular orbitals of the complex are the π (the HOMO and HOMO−1) and σ (HOMO−2) orbitals of the sox-pydx ligand. The lowest unoccupied molecular orbital (LUMO) of the complex is mostly π^* of the sox-pydx ligand (86%) with a small contribution (9%) from the d_{xz}(V) orbital (the Cartesian coordinate system is set up in such a way that the Z axis points along the V−O_{ax} vector and the X axis goes along the O3−O4 direction). The orbital occupancy perturbed Mayer bond order calculations[58c] indicate that the LUMO is a weak antibonding orbital (Table 3). Above the LUMO lie three metal-based orbitals: d_{xy}(V)−p_x(O_{eq}) as LUMO+1, d_{xz}(V)−p_x(O_{ax}) as LUMO+2, and a d_{z^2}-like orbital as LUMO+3. The metal contribution to these orbitals ranges from 63% in LUMO +2 to 73% in LUMO+1, and all three orbitals have antibonding character for the V−O_{ax} and V−O_{eq} interactions (Table 3). The

Table 3. Energies and MPA-Derived Compositions of FMOs of Complex 1 from DFT Calculations

			% contribution			
molecular orbital	description	ε (eV)	V	O_{ax}	O_{eq}	L
LUMO+3	d_{z^2}(V)	−1.40	69.2	9.6	4.7	16.5
LUMO+2	d_{xz}(V)−p_x(O_{ax})	−1.57	63.1	15.5	4.7	16.7
LUMO+1	d_{xy}(V)−p_x(O_{eq})	−1.96	72.9	1.7	15.1	10.3
LUMO	π^*(L) + d_{xz}(V)	−2.53	8.8	3.4	2.1	85.7
HOMO	π(L)	−6.18	1.6	2.3	1.4	94.7
HOMO−1	π(L)	−6.77	0.0	2.8	1.4	95.8
HOMO−2	σ(L)	−7.03	1.7	1.6	3.6	93.1

oxido and sox-pydx ligand contributions of these molecular orbitals reflect on the covalent bonding between the metal and ligands in this complex. As can be expected for $\{VO_2\}^+$ complexes, the V−O_{ax} and V−O_{eq} interactions have the V═O description, and the calculated Mayer bond orders (1.87 for V−O_{ax} and 1.82 for V−O_{eq}) confirm this. The vanadium−sox-pydx ligand covalent interaction is reflected by the V−O3, V−O4, and V−N1 bond orders (0.60, 0.51, and 0.37, respectively), with the V−N1 bond being the weakest metal−ligand interaction in the complex.

The calculated absorption spectrum of complex **1** in solution (Table 4) contains two strong bands at 415 and 329 nm (411

Table 4. Calculated Lowest-Energy Absorption Bands for Complex 1 in Solution from TD-DFT Calculations

λ (nm)	f	assignment	
415	0.102	HOMO → LUMO (92%)	π(L) → π^*(L)
385	0.002	HOMO → LUMO+1 (94%)	π(L) → d_{xy}(V)−p_x(O_{eq})
346	0.015	HOMO−2 → LUMO (78%)	σ(L) → π^*(L)
344	0.064	HOMO−1 → LUMO (52%)	π(L) → π^*(L)
		HOMO → LUMO+2 (21%)	π(L) → d_{xz}(V)−p_x(O_{ax})
329	0.154	HOMO → LUMO+2 (50%)	π(L) → d_{xz}(V)−p_x(O_{ax})
321	0.017	HOMO−1 → LUMO+1 (41%)	π(L) → d_{xy}(V)−p_x(O_{eq})
		HOMO → LUMO+3 (30%)	π(L) → d_{z^2}(V)
319	0.056	HOMO → LUMO+3 (41%)	π(L) → d_{z^2}(V)

and 325 nm in the experimental spectrum in a DMF solution). The lowest-energy absorption is due to the HOMO → LUMO, π(L)→ π^*(L) intraligand electronic excitation. The second strong absorption band near 330 nm is due to the HOMO → LUMO+2, π(L)→ d_{xz}(V)−p_x(O_{ax}) LMCT transition. There are weaker transitions between the first and second strong transitions and near the second strong transition at 329 nm. These bands are expected to contribute to the absorbance in the near-UV region, but they are not expected to show up as distinct bands, being obscured by the stronger bands at 415 and 329 nm (Figure 3).

Electrochemical Studies. In the CV experiments, the vanadium complex **1** shows two ligand-based oxidations at 1.2 and 1.6 V (Figure S10 in the SI): the oxidation at lower potential probably corresponds to oxidation of the phenolate oxygen, whereas at more positive potential, hydrazone-based oxidation occurs. In the zinc(II) complex of the same ligand, irreversible oxidative waves are observed at 0.95 and 1.5 V, supporting the above assignments of the oxidative response of

dx.doi.org/10.1021/ic501216d | Inorg. Chem. 2014, 53, 11426−11437

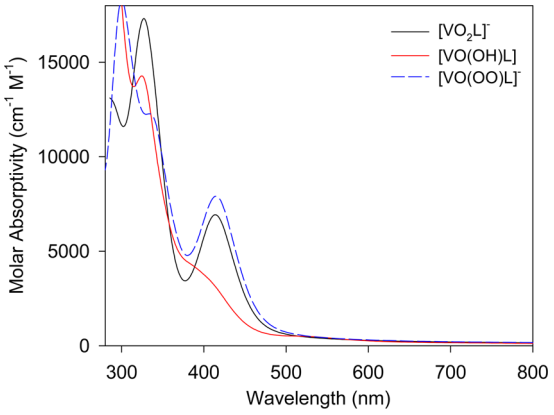

Figure 3. Simulated absorption spectra of complex **1**, [VO(OH)(sox-pydx)], and $[VO(O_2)(sox\text{-}pydx)]^-$ in solution.

complex **1** to ligand-based redox processes. On the negative side of the Ag/AgCl electrode, an irreversible reduction wave was observed at −0.91 V followed by a quasi-reversible reduction wave at −1.45 V, with a peak-to-peak separation of 100 mV. On the basis of the fact that DFT calculations have shown (vide supra) that LUMO is predominantly ligand-centered while LUMO+1 has major contribution from the metal d_{xy} orbital, the first irreversible reduction is assigned to a ligand-centered process, while at more negative potential, the quasi-reversible redox couple is assigned to a vanadium(V)/vanadium(IV) redox pair (Figure 4 and Table 5). Similar results were obtained for a monoanionic dioxidovanadium(V) complex of 5-bromosalicylaldehyde semicarbazone containing vanadium-(V) in an O_4N-donor environment.[62a]

Reaction with HCl. The *cis*-dioxidovanadium(V) complex gives an oxidohydroxo complex upon reaction with acids. The spectral changes observed when 10 μL aliquots of a saturated methanolic solution of HCl were added successively to 2 mL of a 10^{-4} M methanolic solution of $[Et_3NH]$ $[VO_2(sox\text{-}pydx)]$ is depicted in Figure 5. The addition of a HCl solution results in a color change of the complex from yellow to yellowish orange with a slight broadening and decrease in the intensity of the absorption band at 409 nm. Further addition of HCl results in the disappearance of the 294 nm band and the appearance of a new band at 272 nm. An increase in the intensity of the 227 nm band is also observed (Figure 5). It has been established that, upon acidification of the pyridoxal hydrazone complexes of dioxidovanadium(V), an initial protonation takes place at the

Table 5. Electrochemical Data for Complex 1

complex	scan rate	E^0/V (ΔE_p/mV) values from CV	peak potentials (V) in DPV
1	100	1.64, 1.21, −0.90, −1.45 (100)	1.47, 1.14, −0.81, −1.42

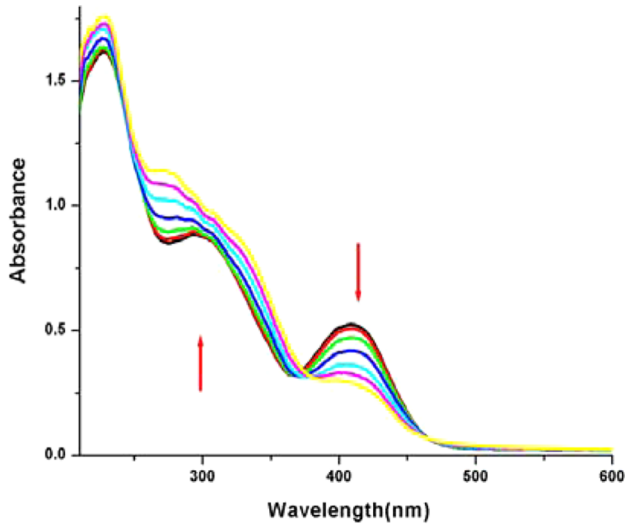

Figure 5. Titration of $[Et_3NH][VO_2(sox\text{-}pydx)]$ with a saturated solution of HCl in methanol. The spectra were recorded after the gradual addition of 10 μL of methanolic HCl to 2 mL of a 1×10^{-4} M methanol solution of $[Et_3NH][VO_2(sox\text{-}pydx)]$.

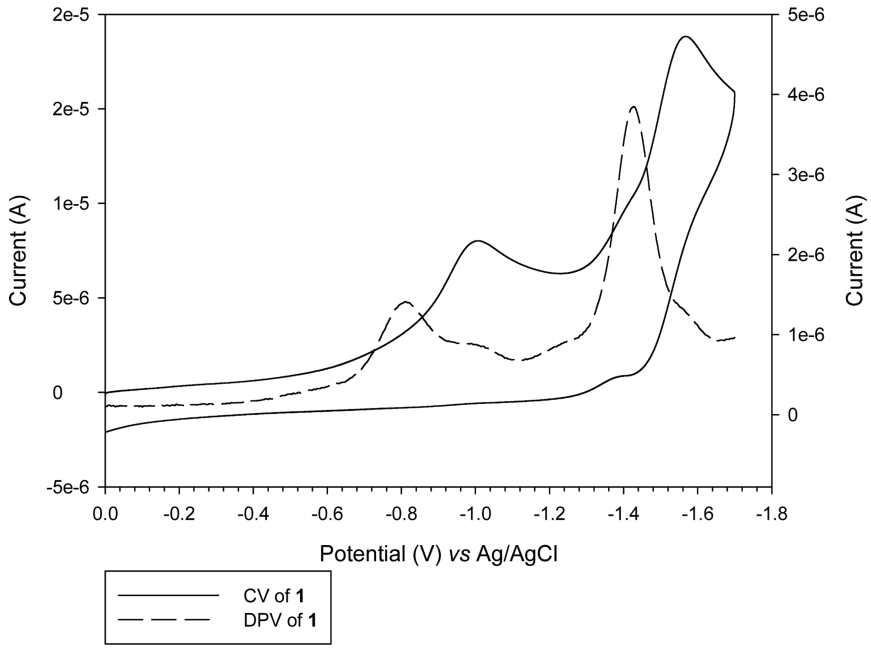

Figure 4. CV and DPV of complex **1** in DMF. For DPV, the current axis is on the right-hand side of the graph.

dx.doi.org/10.1021/ic501216d | *Inorg. Chem.* 2014, 53, 11426−11437

Scheme 2. Protonation of Complex 1

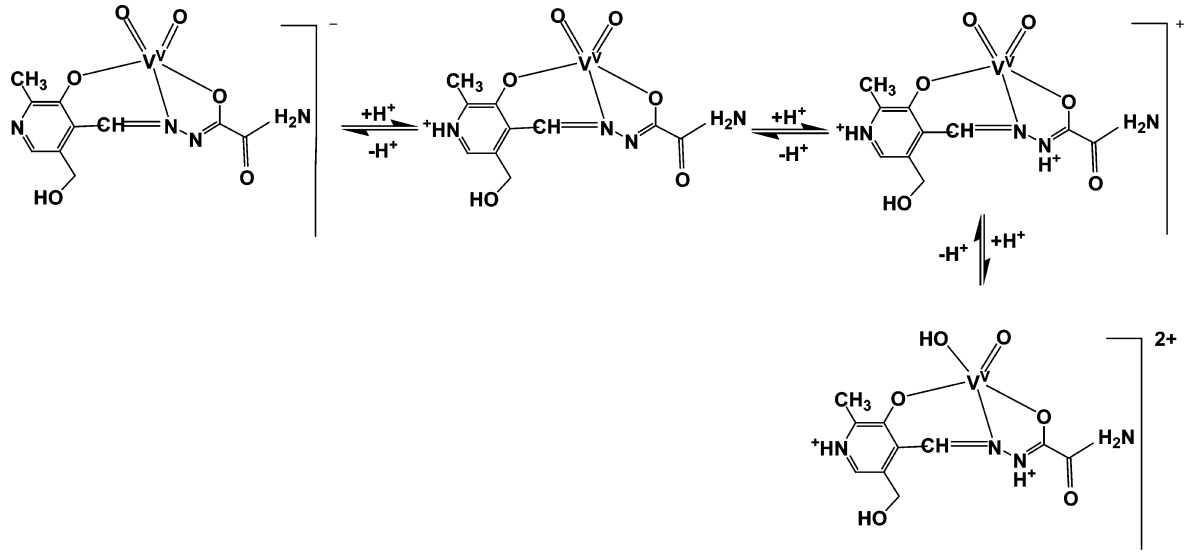

pyridine nitrogen,[45,46,63−65] which is followed by protonation of the hydrazone nitrogen (N2), and finally one of the oxido groups coordinated to vanadium is protonated (Scheme 2).[46] TD-DFT calculation on the hydroxo complex [VO(OH)(sox-pydx)] also points to the effect of protonation on the first strong absorption band at 409 nm (Figure 3). The hydroxo complex has significantly lower absorption intensity in this region relative to the dioxidovanadium(V) complex. Considering that the color change and spectral shifts observed by us are similar to those of previous reports,[45−48] we also assume that the final species formed upon the addition of excess acid to the vanadium complex $[VO_2(sox\text{-}pydx)]^-$ is $[VO(OH)(soxH\text{-}pydxH)]^{2+}$. This transformation is reversible, and the spectra of the parent complex can be regenerated upon the addition of methanolic NaOH (Figure 6). For the catalytic activity of vanadate-dependent haloperoxidase, the presence of a coordinated hydroxo group as well as the reversibility of the dioxido to oxidohydroxo complex conversion is an important observation.[46,65,66] In the protonated complex, the vanadium(V)/vanadium(IV) couple is observed at 30 mV more positive potential than the parent complex (Figure S11 in the SI).

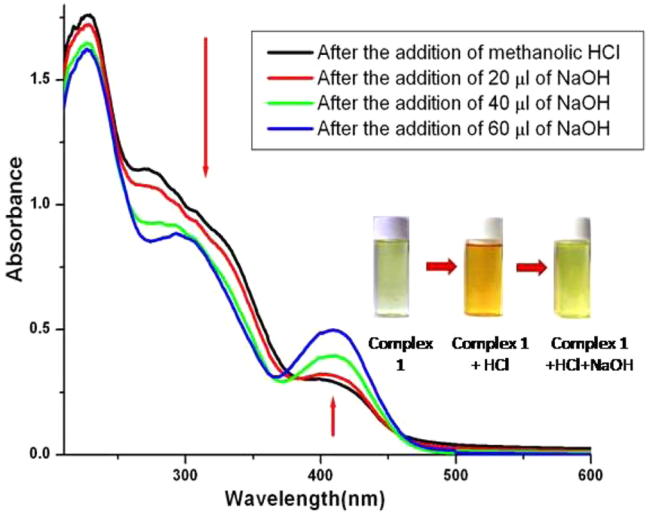

Figure 6. Titration of [VO(OH)(sox-pydx)] (0.5×10^{-4} M) with a saturated solution of NaOH in methanol. The spectra were recorded after the gradual addition of 20 μL of methanolic NaOH.

Reaction with H_2O_2. The addition of H_2O_2 to a methanolic solution of the dioxidovanadium complex leads to formation of the oxidoperoxo complex, which we tentatively assume is $[VO(O_2)(sox\text{-}pydx)]^-$. Although we are unable to isolate the oxidoperoxo complex in the solid state, its formation can be established by absorption spectroscopy (Figure 7) and ESI-MS

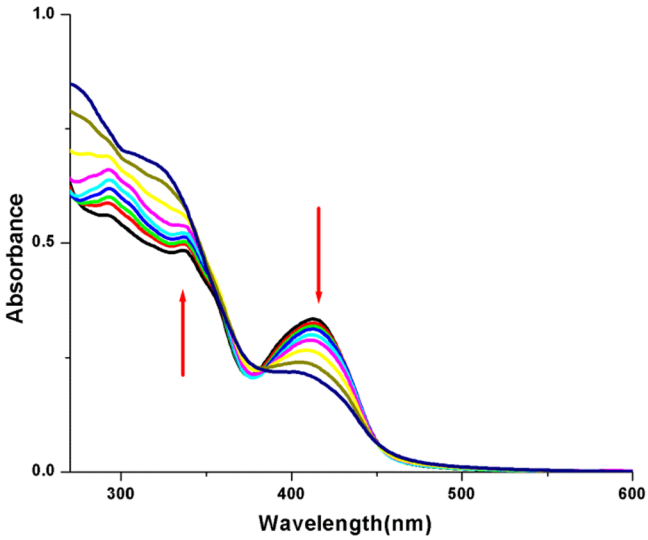

Figure 7. Titration of $[Et_3NH][VO_2(sox\text{-}pydx)]$ with 30% H_2O_2. The spectra were recorded after successive additions of 10 μL of H_2O_2 to 2 mL of a 0.5×10^{-4} M solution of $[Et_3NH][VO_2(sox\text{-}pydx)]$ in methanol.

(Figures S3 and S4 in the SI). The changes recorded in the absorption spectrum after successive additions of 10 μL of 30% H_2O_2 to 2 mL of 0.5×10^{-4} M methanolic $[Et_3NH][VO_2(sox\text{-}pydx)]$ are shown in Figure 7. A slight broadening and decrease in the intensity of the absorption maximum at 409 nm are observed after the addition of H_2O_2. Further addition of H_2O_2 leads to an increase in the intensity of the band at 336 nm along with a blue shift to 324 nm (Figure 7). The ESI-MS spectra (both positive- and negative-ion mode) also show a new peak

dx.doi.org/10.1021/ic501216d | Inorg. Chem. 2014, 53, 11426−11437

Chart 2. Oxidative Bromination of Phenol Red to Bromophenol Blue Catalyzed by 1

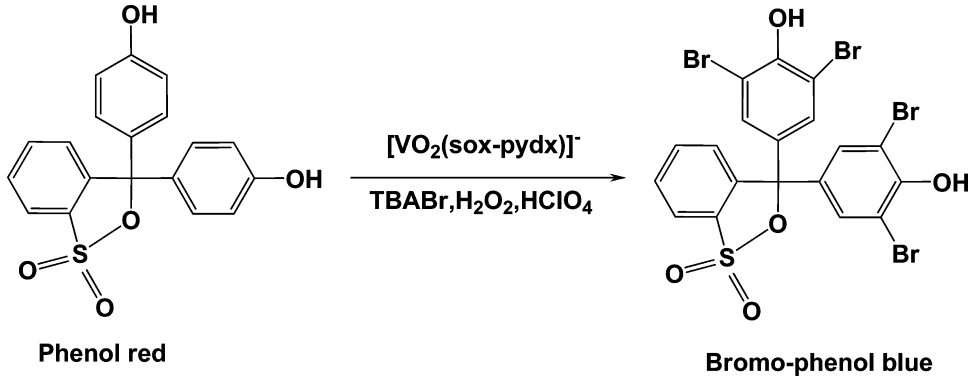

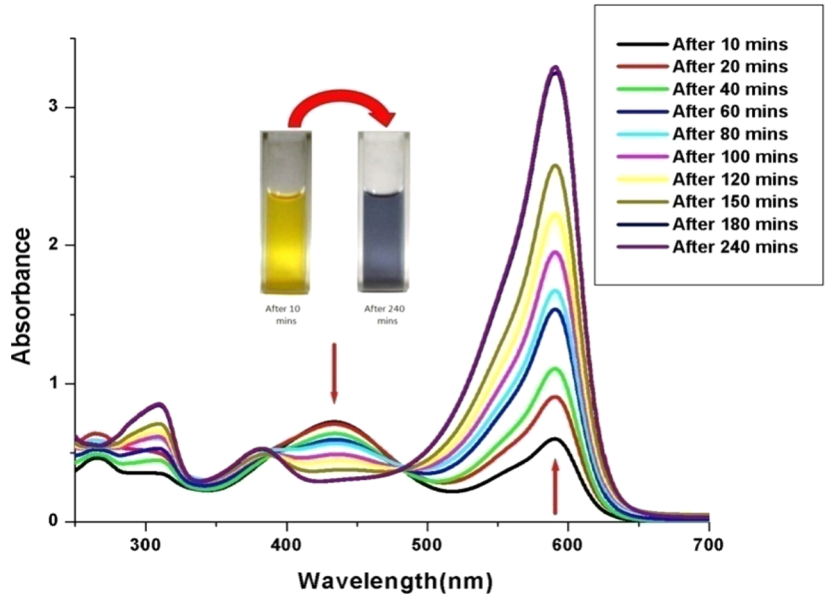

Figure 8. $[Et_3NH][VO_2(sox\text{-}pydx)]$ (0.1 mmol) catalyzed bromination of phenol red (0.25 mmol) followed by absorption spectroscopy. Spectral data taken of aliquots in pH = 7.1 aqueous phosphate buffer.

assignable to $[VO(O_2)(sox\text{-}pydx)]^{\pm}$ (Figures S3 and S4 in the SI). These results can be interpreted in terms of formation of the oxidoperoxo complex of composition $[VO(O_2)(sox\text{-}pydx)]^{-}$.[45−48] We may note here that poor stability in the solid state of peroxo complexes derived from oxido- and dioxidovanadium(V) complexes with pyridoxal hydrazone and thiohydrazone ligands has been reported in the literature.[46,67] We have optimized the structure of the oxidoperoxovanadium-(V) complex using DFT, and the optimized structure is given in Figure S12 in the SI. The η^2-peroxo complex was found to be ∼10 kcal mol^{-1} lower in energy (also a minimum in the PES) than the corresponding η^1-peroxo species.

Catalytic Activity Study. *Oxidative Bromination. a. Conversion of Phenol Red to Bromophenol Blue.* The bromoperoxidase activity of the enzymes as well as their model complexes is often measured by the kinetic study of the catalytic bromination of phenol red to bromophenol blue.[25,31,32]

The catalytic ability of complex **1** for the oxidative bromination of phenol red (Chart 2) was monitored by UV−vis spectrophotometry (Figure 8). The disappearance of the peak due to phenol red at 424 nm and the appearance of a new peak at 590 nm due to bromophenol blue, with isosbestic points at 482 and 389 nm, show clean conversion of phenol red to bromophenol blue, and the reaction was complete after ∼4 h under ambient conditions.

The plots for the kinetic studies of the above conversion are given in Figures 9 and S13 and S14 in the SI. The reaction showed saturation kinetics, and a treatment based on the Michaelis−Menten model originally developed for enzyme kinetics was carried out. The values of the Michaelis binding constant (K_m), maximum velocity (V_{max}), and rate constant for dissociation of substrates (i.e., turnover frequency, k_{cat}) were calculated from the Lineweaver−Burk graph (double reciprocal plot) of 1/rate versus 1/[S] (Figure 9), using the equation $1/V = (K_M/V_{max})(1/[S]) + 1/V_{max}$, and the kinetic parameters are presented in Table 6. The catalytic parameters (K_m,V_{max}, and k_{cat}) were also evaluated by putting the data into the Michaelis−Menten kinetic model using a nonlinear least-squares fitting routine, which gave almost identical values (Table S2 in the SI). A control reaction carried out without the vanadium complex shows no change in the absorbance at 590 nm (Figure S15 in the SI).

b. Bromination of Other Organic Substrates. Oxidative brominations of salicylaldehyde and phenol, catalyzed by the present dioxidovanadium complex (Chart 3), were also studied.

dx.doi.org/10.1021/ic501216d | Inorg. Chem. 2014, 53, 11426−11437

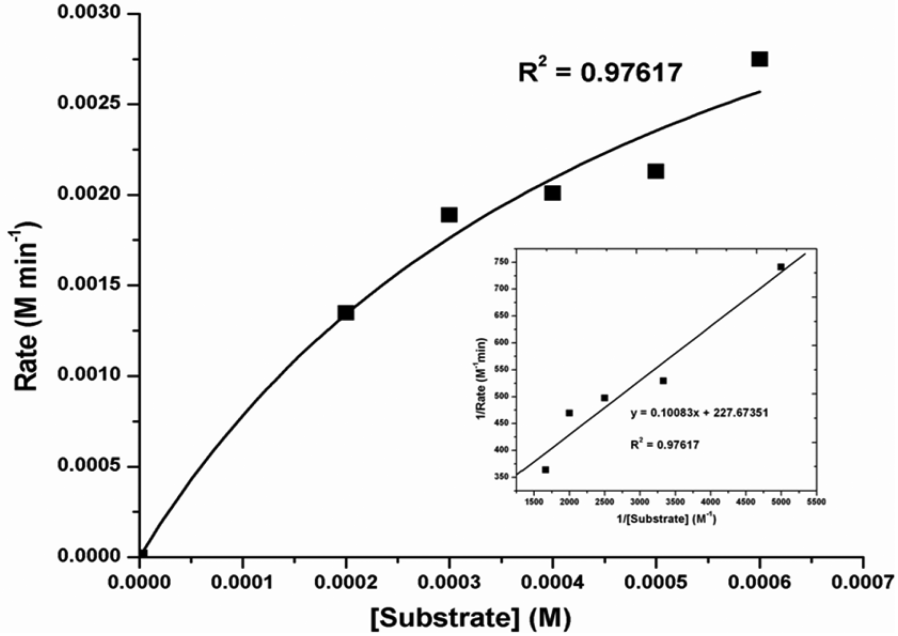

Figure 9. Initial rates versus substrate concentrations for the bromination reaction (Chart 2) catalyzed by complex **1**. The inset shows the Lineweaver–Burk plot.

Table 6. Kinetic Parameters for the Bromination of Phenol Red by Complex 1

V_{max} (M min^{-1})	K_m (M)	k_{cat} (h^{-1})
4.39×10^{-3}	4.4×10^{-4}	26340

In the case of salicylaldehyde, GC analysis revealed the presence of three products in the ratio 71:4:25, with 5-bromosalicylaldehyde as the major product and 3,5-dibromosalicylaldehyde as the other relevant product (4%) along with an unidentified product (25%). For phenol, the selectivity of the formation of *p*-bromophenol was 29% (Table 7). In the absence of the catalyst, no brominated product was obtained from the reaction mixture. Considering the high percentage of substrate conversion, the relatively high selectivity of the formation of 5-bromosalicylaldehyde, the substantially high value of the turnover frequency (TOF), and also the fact that our vanadium complex works in an aqueous medium, it is probably one of the most efficient homogeneous catalysts containing vanadium for oxidative bromination so far reported in the literature.[32,44−46,50,51] A plausible mechanism of the reaction is shown in Scheme 3.

One possible reason for the high catalytic efficiency of complex **1** for the oxidative bromination reaction is probably due to the fact that complex **1** not only has a donor environment around vanadium(V) similar to that of the vanadium-dependent bromoperoxidase enzyme but also has several pendant groups, like hydoxymethyl and amide, that, like the amino acid residues in the enzyme, are capable of stabilizing the catalyst−substrate complex by hydrogen-bonding interactions with the hyrdoxy aromatic substrates (similar to the hydrogen-bonding interactions with Et_3NH^+ in the solid state observed in the X-ray structure). Moreover, from the DFT-optimized structure of the oxidoperoxo complex (Figure S12 in the SI), it is clear that the hydroperoxo intermediate generated during the catalytic cycle (Scheme 3), which is important for increasing the electrophilicity of the peroxido complex, activating the attack by Br^-,[31] may also be stabilized by hydrogen-bonding interactions with either the phenolato or amido oxygen.

Table 7. Bromination of Hydroxyaromatic Compounds Using Complex 1 as a catalyst

substrate	major product	yield (%)	TON[a]	TOF (h^{-1})
salicylaldehyde	5-bromosalicylaldehyde	71	355	88.75
phenol	*p*-bromophenol	29	145	36.25

[a]Time of reaction: 4 h.

Oxidation of Benzene to Phenol. Model complexes showing haloperoxidase activity are also known to catalyze in vitro oxidations of several other organic substrates.[68] The dioxido complex has also been employed to study the oxidation of benzene to phenol (Chart 4). GC analysis revealed that in 18

Chart 3. Oxidative Bromination of Phenol and Salicylaldehyde Catalyzed by Complex 1

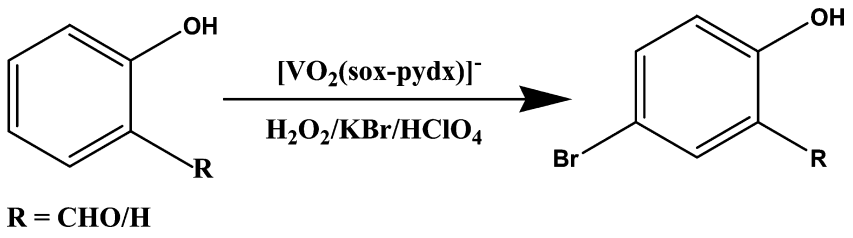

R = CHO/H

dx.doi.org/10.1021/ic501216d | *Inorg. Chem.* 2014, 53, 11426−11437

Scheme 3. Plausible Mechanism of Oxidative Bromination Catalyzed by Complex 1

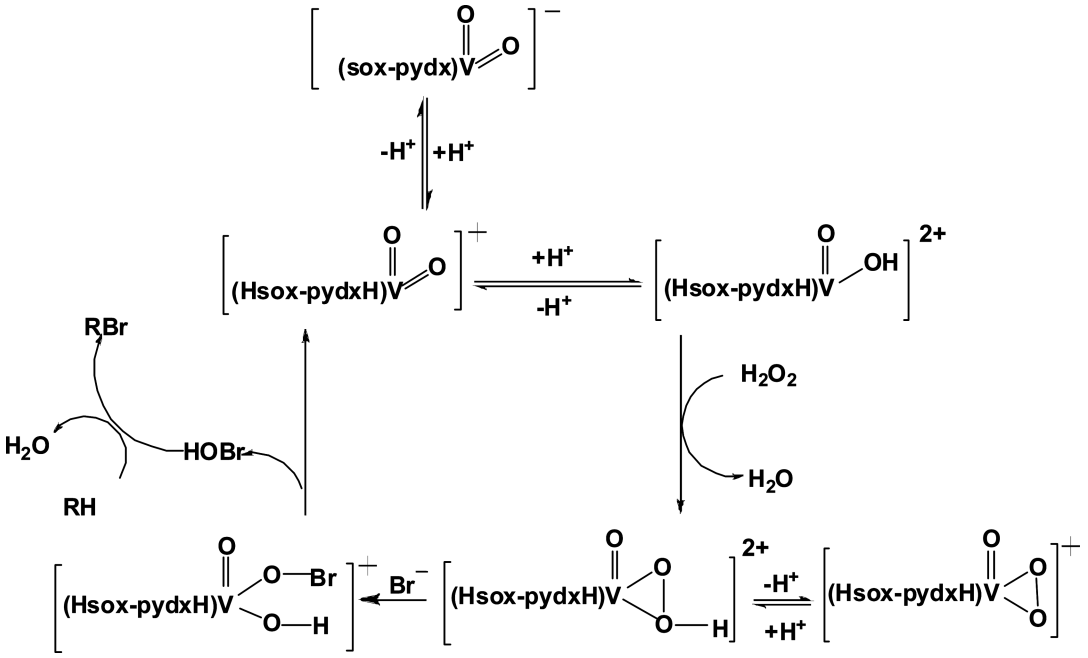

Chart 4. Oxidation of Benzene to Phenol with H_2O_2 Catalyzed by Complex 1

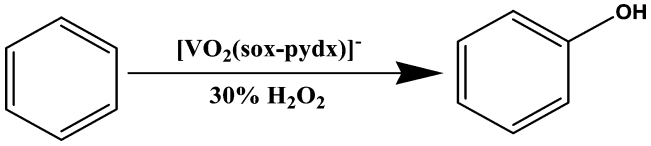

h 78% benzene is converted to phenol. No further oxidation was observed beyond 18 h (Table 8). Again, the high percentage of conversion of the substrate, as well as the high TON and TOF values, indicates that complex **1** is also a very efficient oxidation catalyst for the hydroxylation of aromatic hydrocarbons by H_2O_2.

Table 8. Oxidation of Benzene to Phenol Using Complex 1 as a Catalyst

time (h)	conversion (wt %)	TON	TOF (h^{-1})
3	29	145	48
6	47	235	39
9	72	360	40
18	78	390	22

CONCLUSIONS

Using a new ONO-donor tridentate ligand, we have synthesized a pentacoordinated vanadium(V) complex in an O_4N-donor environment, containing two oxido ligands. The similarity of the coordination environment around vanadium to that of a vanadium-dependent bromoperoxidase enzyme along with the presence of pendant amide and hydroxymethyl groups, which are capable of participating in hydrogen bonding with the peroxo group or substrates, makes the compound a suitable functional model of the enzyme. The compound, in fact, is found to show exceptionally high bromoperoxidase activity, with phenol red as a model substrate, as well as with salicylaldehyde and phenol. It is also able to oxidize benzene to phenol.

ASSOCIATED CONTENT

Supporting Information

X-ray crystallographic data in CIF format, mass, ^{1}H NMR, and IR spectra, FMOs of complex **1**. and other characterization data. This material is available free of charge via the Internet at http://pubs.acs.org.

AUTHOR INFORMATION

Corresponding Authors

*E-mail: sgorelsk@uottawa.ca.

*E-mail: shch20@hotmail.com. Fax: +91 033 2668 2916.

Notes

The authors declare no competing financial interest.

ACKNOWLEDGMENTS

C.D. and P.A. thank the UGC for fellowships, while S.M. thanks the CSIR. S.K.C. acknowledges AICTE for funding the purchase of a CH1106A potentiostat. DST-FIST, UGC-SAP, and MHRD special grants that funded the infrastructural facility created in our department are also thankfully acknowledged. We thank Prof. M. Ali of Jadavpur University for kindly recording the ESI-MS spectra.

REFERENCES

(1) Butler, A. In *Comprehensive Biological Catalysis*; Sinnott, M., Ed.; British Academic Press: Oxford, U.K., 1997; p 427.
(2) Vilter, H. *Met. Ions Biol. Syst.* **1995**, *31*, 325.
(3) Butler, A.; Walker, J. V. *Chem. Rev.* **1993**, *93*, 1937.
(4) Butler, A. In *Bioinorganic Catalysis*; Reedijk, J., Ed.; Marcel Dekker: New York, 1993; p 425.
(5) Wever, R.; Krenn, B. E. Vanadium Haloperoxidases. In *Vanadium in Biological Systems*; Chasteen, N. D., Ed.; Kluwer Academic Publishers: Dordrecht, The Netherlands, 1990; p 81.
(6) Weyand, M.; Hecht, H. J.; Kieß, M.; Liaud, M. F.; Vilter, H.; Schomburg, D. *J. Mol. Biol.* **1999**, *293*, 595.

(7) Isupov, M. I.; Dalby, A. R.; Brindley, A. A.; Izumi, Y.; Tanabe, T.; Murshudov, G. N.; Littlechild, J. A. *J. Mol. Biol.* **2000**, *299*, 1035.
(8) Messerschmidt, A.; Wever, R. *Proc. Natl. Acad. Sci. U.S.A.* **1996**, *93*, 392.
(9) Almeida, M. G.; Humanes, M.; Melo, R.; Silva, J. A.; da Silva, J. J. R. F.; Wever, R. *Phytochemistry* **2000**, *54*, 5.
(10) Almeida, M.; Humanes, M.; Melo, R.; Silva, J. A.; da Silva, J. J. R. F.; Vilter, H.; Wever, R. *Phytochemistry* **1998**, *48*, 229.
(11) Hara, I.; Sakurai, T. *J. Inorg. Biochem.* **1998**, *72*, 23.
(12) Itoh, N.; Izumi, Y.; Yamada, H. *Biochem. Biophys. Res. Commun.* **1985**, *131*, 428.
(13) Palenik, B.; Ren, Q.; Dupont, C.; Myers, G.; Heidelberg, J.; Badger, J.; Madupu, R. *Proc. Natl. Acad. Sci. U.S.A.* **2006**, *103*, 13555.
(14) Johnson, T. L.; Palenik, B.; Brahamsha, B. *J. Phycol.* **2011**, *47*, 792.
(15) Maurya, M. R.; Kumar, A.; Ebel, M.; Rehder, D. *Inorg. Chem.* **2006**, *45*, 5924.
(16) Calviou, L. J.; Arber, J. M.; Collison, D.; Garner, C. D.; Clegg, W. *J. Chem. Soc., Chem. Commun.* **1992**, 654.
(17) Cornman, C. R.; Kampf, J.; Lah, M. S.; Pecoraro, V. L. *Inorg. Chem.* **1992**, *31*, 2035.
(18) Cornman, C. R.; Kampf, J.; Pecoraro, V. L. *Inorg. Chem.* **1992**, *31*, 1981.
(19) Cornman, C. R.; Colpas, G. J.; Hoeschele, J. D.; Kampf, J.; Pecoraro, V. L. *J. Am. Chem. Soc.* **1992**, *114*, 9925.
(20) Keramidas, A. D.; Miller, S. M.; Anderson, O. P.; Crans, D. C. *J. Am. Chem. Soc.* **1997**, *119*, 8901.
(21) Adão, P.; Maurya, M. R.; Kumar, U.; Avecilla, F.; Henriques, R. T.; Kusnetsov, M. L.; Pessoa, J. C.; Correia, I. *Pure Appl. Chem.* **2009**, *81*, 1279.
(22) Rayati, S.; Sadeghzadeh, N.; Khavasi, H. R. *Inorg. Chem. Commun.* **2007**, *10*, 1545.
(23) Wischang, D.; Radlow, M.; Hartung, J. *Dalton Trans.* **2013**, *42*, 11926.
(24) Butler, A. *Coord. Chem. Rev.* **1999**, *187*, 17.
(25) Neidleman, S. L.; Geigert, J. L. *Biohalogenation*; Ellis Horwood Ltd. Press: New York, 1986.
(26) Vergopoulos, V.; Priebsch, W.; Fritzsche, M.; Rehder, D. *Inorg. Chem.* **1993**, *32*, 1844.
(27) Ligtenbarg, A. G. J.; Hage, R.; Feringa, B. L. *Coord. Chem. Rev.* **2003**, *237*, 89.
(28) Rehder, D. *Coord. Chem. Rev.* **1999**, *182*, 297.
(29) Rehder, D.; Santoni, G.; Licini, G. M.; Schulzke, C.; Meier, B. *Coord. Chem. Rev.* **2003**, *237*, 53.
(30) Kimblin, C.; Bu, X.; Butler, A. *Inorg. Chem.* **2002**, *41*, 161.
(31) Colpas, G. J.; Hamstra, B. J.; Kampf, J. W.; Pecoraro, V. L. *J. Am. Chem. Soc.* **1996**, *118*, 3469.
(32) Colpas, G. J.; Hamstra, B. J.; Kampf, J. W.; Pecoraro, V. L. *J. Am. Chem. Soc.* **1994**, *116*, 3627.
(33) Soedjak, H. S.; Butler, A. *Biochemistry* **1988**, *27*, 1629.
(34) Clegue, M. J.; Keder, N. L.; Butler, A. *Inorg. Chem.* **1993**, *32*, 4754.
(35) Butler, A.; Baldwin, A. H. *Struct. Bonding (Berlin)* **1997**, *89*, 109.
(36) Messerschmidt, A.; Prade, L.; Wever, R. *Biol. Chem.* **1997**, *378*, 309.
(37) Messerschmidt, A.; Wever, R. *Inorg. Chim. Acta* **1998**, *273*, 160.
(38) Rehder, D. In *Bioinorganic Vanadium Chemistry*; Wiley: Chichester, U.K., 2008; p 10.
(39) ten Brink, H. B.; Schoemaker, H. E.; Wever, R. *Eur. J. Biochem.* **2001**, *268*, 132.
(40) Bolm, C.; Bienewald, F. *Angew. Chem., Int. Ed. Engl.* **1996**, *34*, 2640.
(41) Santoni, G.; Licini, G. M.; Rehder, D. *Chem.—Eur. J.* **2003**, *9*, 4700.
(42) Smith, T. S.; Pecoraro, V. L. *Inorg. Chem.* **2002**, *41*, 6754.
(43) Conte, V.; Furi, F. D.; Licini, G. *Appl. Catal., A* **1997**, *157*, 335.
(44) de la Rosa, R. I.; Clague, M. J.; Butler, A. *J. Am. Chem. Soc.* **1992**, *114*, 760.
(45) Maurya, M. R.; Agarwal, S.; Bader, C.; Ebel, M.; Rehder, D. *Dalton Trans.* **2005**, 537.
(46) Maurya, M. R.; Agarwal, S.; Bader, C.; Rehder, D. *Eur. J. Inorg. Chem.* **2005**, 147.
(47) Maurya, M. R.; Haldar, C.; Kumar, A.; Kuznetsov, M. L.; Avecilla, F.; Pessoa, J. C. *Dalton Trans.* **2013**, *42*, 11941.
(48) Tótaro, R. M.; Williams, P. A. M.; Apella, M. C.; Blesa, M. A.; Baran, E. J. *J. Chem. Soc., Dalton Trans.* **2000**, 4403.
(49) Si, T. K.; Paul, S. S.; Drew, M. G. B.; Mukherjea, K. K. *Dalton Trans.* **2012**, *41*, 5805.
(50) Patra, S.; Chatterjee, S.; Si, T. K.; Mukherjea, K. K. *Dalton Trans.* **2013**, *42*, 13425.
(51) *SADABS*, version 2.03; Bruker AXS Inc.: Madison, WI, 2002.
(52) Sheldrick, G. M. *Acta Crystallogr., Sect. A* **2008**, *64*, 112.
(53) Frisch, M. J.; Trucks, G. W.; Schlegel, H. B.; Scuseria, G. E.; Robb, M. A.; Cheeseman, J. R.; Scalmani, G.; Barone, V.; Mennucci, B.; Petersson, G. A.; Nakatsuji, H.; Caricato, M.; Li, X.; Hratchian, H. P.; Izmaylov, A. F.; Bloino, J.; Zheng, G.; Sonnenberg, J. L.; Hada, M.; Ehara, M.; Toyota, K.; Fukuda, R.; Hasegawa, J.; Ishida, M.; Nakajima, T.; Honda, Y.; Kitao, O.; Nakai, H.; Vreven, T.; Montgomery, J. A., Jr.; Peralta, J. E.; Ogliaro, F.; Bearpark, M.; Heyd, J. J.; Brothers, E.; Kudin, K. N.; Staroverov, V. N.; Kobayashi, R.; Normand, J.; Raghavachari, K.; Rendell, A.; Burant, J. C.; Iyengar, S. S.; Tomasi, J.; Cossi, M.; Rega, N.; Millam, N. J.; Klene, M.; Knox, J. E.; Cross, J. B.; Bakken, V.; Adamo, C.; Jaramillo, J.; Gomperts, R.; Stratmann, R. E.; Yazyev, O.; Austin, A. J.; Cammi, R.; Pomelli, C.; Ochterski, J. W.; Martin, R. L.; Morokuma, K.; Zakrzewski, V. G.; Voth, G. A.; Salvador, P.; Dannenberg, J. J.; Dapprich, S.; Daniels, A. D.; Farkas, Ö.; Foresman, J. B.; Ortiz, J. V.; Cioslowski, J.; Fox, D. J. *Gaussian 09*, revision A.02; Gaussian Inc.: Wallingford, CT,2009.
(54) (a) Becke, A. D. *J. Chem. Phys.* **1993**, *98*, 5648. (b) Lee, C.; Yang, W.; Parr, R. G. *Phys. Rev. B* **1988**, *37*, 785.
(55) Schafer, A.; Huber, C.; Ahlrichs, R. *J. Chem. Phys.* **1994**, *100*, 5829.
(56) Marenich, A. V.; Cramer, C. J.; Truhlar, D. G. *J. Phys. Chem. B* **2009**, *113*, 6378.
(57) Reed, A. E.; Weinstock, R. B.; Weinhold, F. *J. Chem. Phys.* **1985**, *83*, 735.
(58) (a) Mulliken, R. S. *J. Chem. Phys.* **1955**, *23*, 1833. (b) Mayer, I. *Theor. Chim. Acta* **1985**, *67*, 315. (c) Gorelsky, S. I. *J. Chem. Theory Comput.* **2012**, *8*, 908. (d) Gorelsky, S. I. *AOMix: Program for Molecular Orbital Analysis*; University of Ottawa: Ottawa, Canada, 2014; http://www.sg-chem.net/. (e) Gorelsky, S. I.; Lever, A. B. P. *J. Organomet. Chem.* **2001**, *635*, 187.
(59) Gorelsky, S. I. *SWizard program*; University of Ottawa: Ottawa, Canada, 2013; http://www.sg-chem.net/.
(60) (a) Naskar, S.; Naskar, S.; Figgie, H. M.; Sheldrick, W. S.; Chattopadhyay, S. K. *Polyhedron* **2010**, *29*, 493. (b) Naskar, S.; Naskar, S.; Butcher, R. J.; Chattopadhyay, S. K. *Inorg. Chim. Acta* **2010**, *363*, 404.
(61) Addison, A. W.; Rao, T. N.; Reedijk, J.; van Rijn, J.; Verschoor, G. C. *J. Chem. Soc., Dalton Trans.* **1984**, 1349.
(62) (a) Noblía, P.; Vieites, M.; Parajón-Costa, B. S.; Baran, E. J.; Cerecetto, H.; Draper, P.; González, M.; Piro, O. E.; Castellano, E. E.; Azqueta, A.; de Ceráin, A. L.; Monge-Vega, A.; Gambino, D. *J. Inorg. Biochem.* **2005**, *99*, 443. (b) Dutta, S.; Basu, P.; Chakravorty, A. *Inorg. Chem.* **1993**, *32*, 5343. (c) Nikolakis, V. A.; Exarchou, V.; Jakusch, T.; Woolins, J. D.; Slawin, A. M. Z.; Kiss, T.; Kabanos, T. A. *Dalton Trans.* **2010**, *39*, 9032. (d) Nikolakis, V. A.; Tsalavoutis, J. T.; Stylianou, M.; Evgeniou, E.; Jakusch, T.; Melman, A.; Sigalas, M. P.; Kiss, T.; Keramidas, A. D.; Kabanos, T. A. *Inorg. Chem.* **2008**, *47*, 11698.
(63) Plass, W. *Coord. Chem. Rev.* **2003**, *237*, 205.
(64) Maurya, M. R.; Khurana, S.; Shailendra; Azam, A.; Zhang, W.; Rehder, D. *Eur. J. Inorg. Chem.* **2003**, 1966.
(65) Maurya, M. R.; Kumar, A.; Abid, A.; Azam, A. *Inorg. Chim. Acta* **2006**, *359*, 2439.
(66) Keppler, B. K.; Frissen, C.; Moritz, H. G.; Vongorichten, H.; Vogil, E. *Struct. Bonding (Berlin)* **1991**, *78*, 97.

(67) Maurya, M. R.; Kumar, A.; Bhat, A. R.; Azam, A.; Bader, C.; Rehder, D. *Inorg. Chem.* **2006**, *45*, 1260.
(68) Schmidt, H.; Bashirpoor, M.; Rehder, D. *J. Chem. Soc., Dalton Trans.* **1996**, 3865.